Proceedings of 20th International Congress on Acoustics, ICA 2010

23-27 August 2010, Sydney, Australia

FDTD modelling of frequency dependent boundary conditions for room acoustics

Hyok Jeong and Yiu Wai Lam

Acoustics Research Centre, University of Salford, Salford M5 4WT, UK

PACS: 43.55.Ka, 43.55.Ev

ABSTRACT

FDTD has become a popular tool in acoustic modelling in recent years. A main attraction of FDTD is that it can be implemented in computer code easily using simple straightforward marching algorithms and finite difference equations. However, this simplicity comes at a price. Dispersion errors, source scattering, and frequency dependent boundary reflections are just a few of the problems that FDTD has to deal with. Generally the former two are artificial problems of the numerical scheme. The last one, however, is a key component in any room acoustics applications. In theory, the boundary condition can be presented as an impulse response to be convoluted with the FDTD update equations. Unfortunately, this is a rather time consuming process. There are various approximations that can be used to represent a frequency dependent boundary condition in the time domain to speed up the calculation, but their suitability for room acoustics applications has rarely been properly validated. In particular, a practical problem faced in real room acoustics application is that full bandwidth data on a boundary's impedance value is rarely available. In fact, in most cases one may only have information on the absorption coefficient of the boundary in octave frequency bands. Hence it will be of interest to see if an approximation based on the absorption coefficient alone can be used in a FDTD scheme to produce acceptable results. The purpose of this paper is to compare different ways of modelling frequency dependent boundary condition in a FDTD scheme to predict the sound field in a room. In this study, the accuracy of these methods will be validated against calculations by the more accurate boundary element method to assess their applicability in terms of room acoustics criteria.

INTRODUCTION

Modelling of frequency dependent boundary conditions in the FDTD method has received much attention recently since it is a key feature for room acoustic simulation over others such as source scattering, dispersion problem and so on. To implement proper frequency dependent boundary conditions in a time domain method, we first require a representation of the acoustical properties of common wall surfaces such as porous materials, commonly defined in terms of impedance, reflection coefficient or absorption coefficient. Since most of these quantities are defined or measured in the frequency domain, we will need to determine how to approximate these data in the time domain, and to consider the various possibilities of implementing them in a time domain method. Here, we studied several ways of approximating and implementing different types of acoustical properties of porous materials [1-7]. Once the data of the materials are approximated, they are formulated as a digital filter in the z-domain using a bilinear transform. For the implementation, two different approaches were applied – one based on the impedance and the other based on the reflection coefficient of the surface. The FDTD implementations of the frequency dependent boundary conditions will be validated with results from a boundary element method (BEM). The spectrum of the point-received impulse response in a three dimensional setting will be used for the validation. The comparison between the different implementations will be discussed using both frequency responses and room acoustics parameters to determine their usability.

THEORITICAL FORMULATIONS

Basic Equaions

In room acoustic simulation, a FDTD method models the sound propagation using a finite difference scheme in time and space. The first order Euler and Continuity differential equations are the basic equations for the conventional leap-frog FDTD method.

$$Euler\ equation: \frac{\partial \mathbf{v}}{\partial t} = -\frac{1}{\rho_0}\nabla p,$$

$$Continuity\ equation: \frac{\partial p}{\partial t} = -\rho_0 c^2 \nabla \cdot \mathbf{v} \qquad \textbf{(1)}$$

where where p is the sound pressure, $\boldsymbol{v}$ is the particle velocity vector. Because of their interdependence, the sound pressure and particle velocities need to be calculated alternatively in a staggered grid. The resulting 3D FDTD equations can be written in a Cartesian grid as follows.

$$v_x^{n+\frac{1}{2}}\left(i+\tfrac{1}{2},j,k\right) = v_x^{n-\frac{1}{2}}\left(i+\tfrac{1}{2},j,k\right) - \frac{\Delta t}{\rho_0 \Delta x}\left[p^n(i+1,j,k) - p^n(i,j,k)\right]$$

$$v_y^{n+\frac{1}{2}}\left(i,j+\tfrac{1}{2},k\right) = v_y^{n-\frac{1}{2}}\left(i,j+\tfrac{1}{2},k\right) - \frac{\Delta t}{\rho_0 \Delta x}\left[p^n(i,j+1,k) - p^n(i,j,k)\right]$$

$$v_z^{n+\frac{1}{2}}\left(i,j,k+\tfrac{1}{2}\right) = v_z^{n-\frac{1}{2}}\left(i,j,k+\tfrac{1}{2}\right) - \frac{\Delta t}{\rho_0 \Delta x}\left[p^n(i,j,k+1) - p^n(i,j,k)\right] \quad \textbf{(2)}$$

$$p^{n+1}(i,j,k) = p^n(i,j,k) - \frac{\rho_0 c^2 \Delta t}{\Delta x}\left[v_x^{n+\frac{1}{2}}\left(i+\tfrac{1}{2},j,k\right) - v_x^{n+\frac{1}{2}}\left(i-\tfrac{1}{2},j,k\right)\right] - \frac{\rho_0 c^2 \Delta t}{\Delta y}\left[v_y^{n+\frac{1}{2}}\left(i,j+\tfrac{1}{2},k\right) - v_y^{n+\frac{1}{2}}\left(i,j-\tfrac{1}{2},k\right)\right] - \frac{\rho_0 c^2 \Delta t}{\Delta y}\left[v_y^{n+\frac{1}{2}}\left(i,j+\tfrac{1}{2},k\right) - v_y^{n+\frac{1}{2}}\left(i,j-\tfrac{1}{2},k\right)\right] \quad \textbf{(3)}$$

For propagation in a Cartesian grid, numerical stability is ensured if

$$\Delta t \leq \frac{1}{c\sqrt{\frac{1}{\Delta x^2}+\frac{1}{\Delta y^2}+\frac{1}{\Delta z^2}}} \quad \textbf{(4)}$$

This equation is related to the parameter known as Courant number and its development is well documented in [8] for acoustical cases. In addition, the cell grid has to be small enough to track the spatial variations of the excitation signal. Additionally, propagating the sound field in rectangular steps creates dispersion errors, which can be kept small by using a small grid size, a high order central difference scheme, or a spectral decomposition method. Here a small grid size is used. As a general rule [9], it is recommended that the size of the cell grid should be smaller than at least *λ/20* of the higher frequency of interest when a first order central difference scheme is used.

Source implementation

The source signal implemented in the calculation is a Gaussian pulse.

$$\mathrm{S}(t) = \mathrm{A}e^{(-\sigma \cdot t)^2} \quad \textbf{(5)}$$

This gives a broadband Gaussian frequency spectrum that can be adjusted through the parameter σ. A hard source is implemented simply by specifying the field at the source node with the specified source, or driving function. The hard source implementation is as follows

$$p_{src}{}^n(i,j,k) = f^n \quad \textbf{(6)}$$

The hard source will scatter the returning waves in an artificial way. It is possible to implement a transparent source to eliminate the source scattering. However, the implementation of a proper transparent source is not computationally efficient. We will show later that a simple filtering procedure can be used to remove the hard source effect efficiently.

MODELLING OF FREQUENCY DEPENDENT BOUNDARY CONDITIONS

Approximation of different data formats

As mentioned before, the acoustical properties of wall materials can be represented in different ways. In this section, two different approximations, which are used to represent the impedance and the reflection coefficient of a boundary will be explained.

2-DOF approximation

The acoustic impedance of common room boundary can be approximated by a one or multi degree of freedom system [3, 7], at least in a limited frequency band. A 2-DOF approximation is particularly effective in the low to medium frequency range (up to 500 Hz in our cases) for a porous surface. The impedance of a 2-DOF system can be written as:

$$Z(\omega) = \frac{p}{v} = j\omega M_{b1} + B_{b1} + \frac{K_{b1}}{j\omega} - \frac{\frac{{K_{b1}}^2}{j\omega}}{-M_{b2}\omega^2 + j\omega B_{b2} + K_{b1} + K_{b2}} \quad \textbf{(7)}$$

By choosing proper values of the system (*M*'s, *B*'s, *K*'s), normal impedance of the boundary can be approximated. A general frequency-domain impedance condition can be formulated for time domain applications via the z-domain using the bilinear approximation [6], $Z(j\omega) \rightarrow 2f_s\left(\frac{\mathrm{Z}-1}{\mathrm{Z}+1}\right)$

Using the bilinear approximation, the impedance condition (7) can be expressed in the z-domain as

$$Z(\mathrm{z}) = M_{b1}2f_s\left(\frac{\mathrm{Z}-1}{\mathrm{Z}+1}\right) + B_{b1} + \frac{K_{b1}}{2f_s}\left(\frac{\mathrm{Z}+1}{\mathrm{Z}-1}\right) - \frac{\frac{{K_{b1}}^2}{2f_s}\left(\frac{\mathrm{Z}+1}{\mathrm{Z}-1}\right)}{M_{b2}4{f_s}^2\left(\frac{\mathrm{Z}-1}{\mathrm{Z}+1}\right)^2 + B_{b2}2f_s\left(\frac{\mathrm{Z}-1}{\mathrm{Z}+1}\right) + K_{b1}+K_{b2}} \quad \textbf{(8)}$$

Minimum phase approximation

If only the magnitude of a reflection coefficient is to be approximated by a filter, it can be done simply by modern optimisation methods such as least p-th norm, with the phase constrained simply by linear phase or minimum phase approximation etc. Once the magnitude of the reflection coefficient is approximated, the simple relation at normal incidence:

$$\left(Z(\mathrm{z}) = \frac{1+R(\mathrm{z})}{1-R(\mathrm{z})}\rho_0 c, for\ \theta = 0\right)$$

can be used to calculate the equivalent surface impedance. Obviously this is only true for normal incidence, but it will be interesting to see if the error can be somewhat compensated when the random incidence absorption coefficient is used to calculated the reflection coefficient magnitude. Furthermore, the phase is not going to be accurate since it is approximated only by a linear or minimum phase requirement.

The reason for looking at using the magnitude of a reflection coefficient together with a minimum phase approximation is that the magnitude of reflection coefficient can be derived by the simple equation

$$\left(|\mathrm{R}| = \sqrt{1-\alpha}\right)$$

In practice, the most common acoustical data available on room boundaries are typical only the random incidence absorption coefficient. Therefore it will be useful to see if one can derive an approximate time domain boundary condition based on such simple data. To maintain consistence in our numerical tests, the surface impedance is fixed first. For the reflection coefficient approach, the random incidence absorption coefficient is then derived from the surface impedance using Paris' formula. The magnitude of the reflection coefficient is then approximated by least p-th norm, and then the phase is approximated by a minimum phase algorithm. It can then be implemented directly in the FDTD using a reflection approach, or converted into impedance for the impedance approach.

Implementation of the boundary condition in z-domain

Impedance approach

It was shown in the previous section that the boundary condition can be expressed in the z-domain by the 2-DOF or minimum phase approximation. The z-transform of the impedance can be modelled in general by

$$Z(z) = \frac{b_1 + \sum_{k=2}^{K} b_k Z^{k-1}}{1 + \sum_{l=2}^{L} a_l Z^{l-1}} \tag{9}$$

where *a*'s and *b*'s are the constants that give the best approximation to the impedance.

For example, the impedance condition (8) can be rearranged as

$$Z(\mathrm{z}) = \frac{b_1 + b_2\mathrm{Z}^{-1} + b_3\mathrm{Z}^{-2} + b_4\mathrm{Z}^{-3} + b_5\mathrm{Z}^{-4}}{1 + a_2\mathrm{Z}^{-1} + a_3\mathrm{Z}^{-2} + a_4\mathrm{Z}^{-3} + a_5\mathrm{Z}^{-4}} \tag{10}$$

For positive x direction, the impedance condition in the absence of flow is given by

$$P(z) = Z(\mathrm{z})V(\mathrm{z}) \tag{11}$$

where *P(z)* is the z-transform of the acoustic pressure, *Z(z)* is the z-transform of the impedance, and *V(z)* is the z-transform of the acoustic normal velocity at the boundary.

By substituting equation (10) into (11) and performing the inverse z-transform of that, we obtain

$$\begin{aligned} p^n = &-a_2 p^{n-1} - a_3 p^{n-2} - a_4 p^{n-3} - a_5 p^{n-4} + b_1 v^n \\ &+ b_2 v^{n-1} + b_3 v^{n-2} + b_4 v^{n-3} \\ &+ b_5 v^{n-4} \end{aligned} \tag{12}$$

where the superscript *n* indicates the time level.

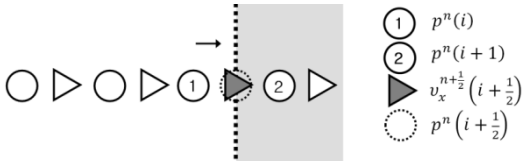

Figure 1 Pressure and velocity nodes near the boundary (positive x direction in 1D)

As shown in Fig. 1, in 1D FDTD, the update equation for velocity node of the boundary can be expressed as

$$\begin{aligned} v_x^{n+\frac{1}{2}}\left(i+\frac{1}{2}\right) = &\ v_x^{n-\frac{1}{2}}\left(i+\frac{1}{2}\right) \\ &- \frac{2\Delta t}{\rho_0 \Delta x}\left[p^n\left(i+\frac{1}{2}\right) - p^n(i)\right] \end{aligned} \tag{13}$$

Since the pressure $p^n(i+½)$ is the unknown variable, a linear interpolation is used to express it as a function of $p^{n+½}(i+½)$ and $p^{n-½}(i+½)$.

Then, applying the difference equation (12) into the unknown pressure node, the equation can be solved for $v_x^{n+½}(i+½)$

$$\begin{aligned} &v_x^{n+\frac{1}{2}}\left(i+\frac{1}{2}\right) \\ &= \frac{v_x^{n-\frac{1}{2}}\left(i+\frac{1}{2}\right) - \frac{\Delta t}{\rho_0 \Delta x}\left(-a_2 p^{n-\frac{1}{2}}\left(i+\frac{1}{2}\right) - (a_2+a_3)p^{n-\frac{3}{2}}\left(i+\frac{1}{2}\right)\right.}{1+\frac{b_1 \Delta t}{\rho_0 \Delta x}} \\ &\frac{-(a_3+a_4)p^{n-\frac{5}{2}}\left(i+\frac{1}{2}\right) - (a_4+a_5)p^{n-\frac{7}{2}}\left(i+\frac{1}{2}\right) - a_5 p^{n-\frac{9}{2}}\left(i+\frac{1}{2}\right)}{1+\frac{b_1 \Delta t}{\rho_0 \Delta x}} \\ &\frac{+(b_1+b_2)v_x^{n-\frac{1}{2}}\left(i+\frac{1}{2}\right) + (b_2+b_3)v_x^{n-\frac{3}{2}}\left(i+\frac{1}{2}\right) + (b_3+b_4)v_x^{n-\frac{5}{2}}\left(i+\frac{1}{2}\right)}{1+\frac{b_1 \Delta t}{\rho_0 \Delta x}} \\ &\frac{\left.+(b_4+b_5)v_x^{n-\frac{7}{2}}\left(i+\frac{1}{2}\right) + b_5 v_x^{n-\frac{9}{2}}\left(i+\frac{1}{2}\right)\right) + \frac{2\Delta t}{\rho_0 \Delta x}p^n(i)}{1+\frac{b_1 \Delta t}{\rho_0 \Delta x}} \end{aligned} \tag{14}$$

Reflection coefficient approach

Recalling eq. (13), and using the interpolation explained in the previous section, the update equation for velocity node of the boundary can be expressed by the following

$$v_x^{n+\frac{1}{2}}\left(i+\frac{1}{2}\right) = \frac{\left(1-\frac{c\Delta t}{\Delta x}\right)v_x^{n-\frac{1}{2}}\left(i+\frac{1}{2}\right) + \frac{2\Delta t}{\rho_0 \Delta x}p^n(i)}{1+\frac{c\Delta t}{\Delta x}} \tag{15}$$

Reflection coefficient also can be expressed in z-domain by either the 2-DOF or minimum phase approximation in the

form of eq. (9). For example, if we use a 4th order filter the reflection coefficient in z-domain can be expressed as

$$R(\mathrm{z}) = \frac{V(\mathrm{z})_{ref}}{V(\mathrm{z})_{inc}} = \frac{b_1 + b_2\mathrm{Z}^{-1} + b_3\mathrm{Z}^{-2} + b_4\mathrm{Z}^{-3} + b_5\mathrm{Z}^{-4}}{1 + a_2\mathrm{Z}^{-1} + a_3\mathrm{Z}^{-2} + a_4\mathrm{Z}^{-3} + a_5\mathrm{Z}^{-4}} \quad \textbf{(16)}$$

The difference equation of the boundary is obtained by re-arranging the equations to

$$\begin{aligned} & v_x^{n+\frac{1}{2}}\left(i+\tfrac{1}{2}\right)_{ref} \\ &= b_1 v_x^{n+\frac{1}{2}}\left(i+\tfrac{1}{2}\right)_{inc} + b_2 v_x^{n-\frac{1}{2}}\left(i+\tfrac{1}{2}\right)_{inc} + b_3 v_x^{n-\frac{3}{2}}\left(i+\tfrac{1}{2}\right)_{inc} \\ &+ b_4 v_x^{n-\frac{5}{2}}\left(i+\tfrac{1}{2}\right)_{inc} + b_5 v_x^{n-\frac{7}{2}}\left(i+\tfrac{1}{2}\right)_{inc} - a_2 v_x^{n-\frac{1}{2}}\left(i+\tfrac{1}{2}\right)_{ref} \\ &- a_3 v_x^{n-\frac{3}{2}}\left(i+\tfrac{1}{2}\right)_{ref} - a_4 v_x^{n-\frac{5}{2}}\left(i+\tfrac{1}{2}\right)_{ref} - a_5 v_x^{n-\frac{7}{2}}\left(i+\tfrac{1}{2}\right)_{ref} \end{aligned} \quad \textbf{(17)}$$

In order to match the continuous frequency to the discrete frequency, the filter has to be pre-warped,

$$\omega_{d,res} = 2f_s tan\left(\frac{\omega_{res}}{2f_s}\right)$$

replaces ω_{res} in the equations for the zeros and poles. For the difference equation (17), it should be noticed that the velocity node in FDTD computational domain contains the information about both the incident and reflected pulse. Therefore, the incident velocity needs to be extracted and entered into the equation. Although we explained the implementing of boundary conditions only for the positive *x* direction in one dimensional case for convenience, it can be easily expanded to three dimensions by considering the normal velocity vector for the negative direction and by extending the arguments for the other spatial directions by adding further dimensional indexes such as *j* and *k*.

NUMERICAL RESULTS

Listening room setting

As shown in Fig 2, the computational grid used in the numerical calculation was 6.9m 4.6m 2.8m [10] having $\Delta x = \Delta y = \Delta z = 2cm$. The source and receiver positions are depicted in Figure 2. The size of the cell grid is directly related to the dispersion errors and could affect stair-case approximation errors when tilted boundary is used in the room of interest. Therefore, in our study, we modelled simple rectangular box type listening room in order to keep away from the effect of the stair-case problem. In addition, the size of the cell grid was carefully chosen to satisfy the criterion ($<\lambda/20$) to avoid the dispersion problem. The size of the cell used in the calculation was smaller than the recommended size for the highest frequency of our interest. It was found that the size of the cell is valid up to 500Hz in the frequency domain. The impulse response at each receiver point was calculated up to 0.8 second in time domain using a $\Delta t = 0.00002s$.

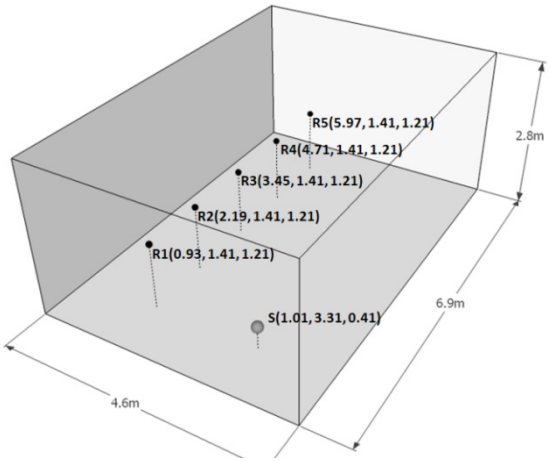

Figure 2 Configuration of the listening room

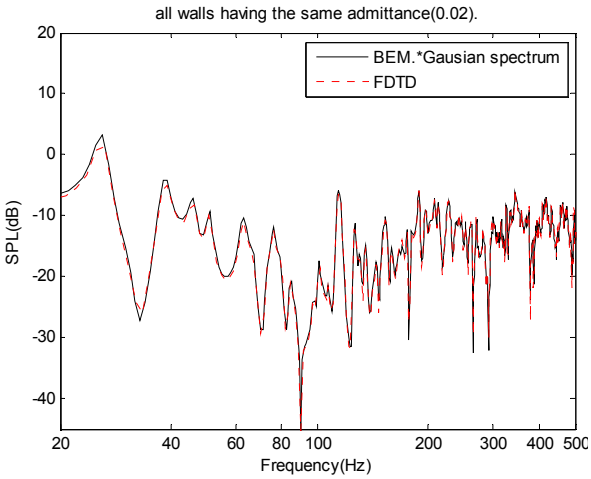

Figure 3 Frequency response at R4

Simple test for hard source effect

When a hard source is implemented, since the update equations do not apply to the source node, its value is fixed solely by the driving function. One may simply suspect that it could work as a scattered object. However, when a Gaussian pulse is generated, it was observed that not only it scattered any field incident upon it, it also introduced numerically artificial effects throughout the entire computational domain especially at low frequencies. Big ripples are easily observed in the calculated impulse response at any receiver point when a hard source is implemented. In this context, a simple validation test to check the effect of the hard source was carried out. As a trial to remove it, proper truncation of the impulse response and high pass filter were applied to the impulse response. As shown in Fig. 3, the effect of the hard source was efficiently removed. It was found that, with proper digital signal processing, a simple hard source implementation can be used effectively in a 3D FDTD simulation. For the test shown in Fig. 3, a frequency independent boundary condition [11] was applied to all walls in the room with a constant admittance value ($\beta = 0.02$). For the comparison, the Gaussian spectrum was multiplied to the result of a boundary element method in frequency domain. The FDTD and BEM results are then compared in the frequency domain. It can be seen that the two are virtually identical.

Results for different boundary conditions in 3D

In this section, various combinations of the approximations and implementations explained in the theorey sections are compared to the boundary element method. Various frequency dependent surface impedance data were obtained using the Delany-Bazley impedance model (DB model) to test the accuracy of the different methods under different conditions. Both the magnitude and phase of the impedance can be controlled by variables of the model such as resistivity and depth [12]. 4 different cases of the listening room were tested with different boundary conditions (Table 1, Fig 4).

Table 1. listening room setting with different condition

Cases	Material settings for different boundaries
Case 1	All the walls: DB model (150KPa/m^2, 50mm)
Case 2	All the walls: DB model (32KPa/m^2 , 100mm)
Case 3	Only floor: DB model (2KPa/m^2, 200mm), others : admittance 0.001
Case 4	All the walls: DB model (2KPa/m^2, 200mm)

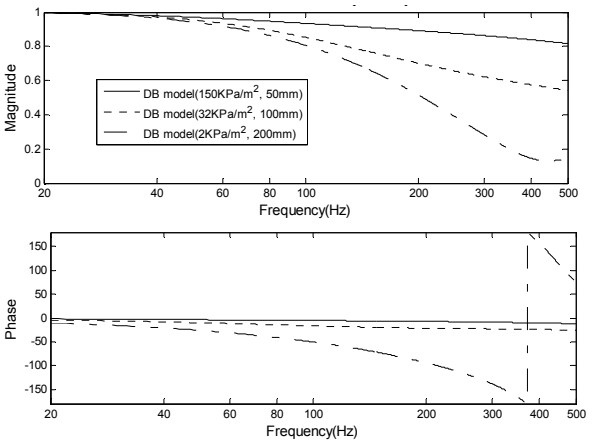

Figure 4 Reflection coefficient of the Delaney-Bazley model used in the listening room setting

The different boundary conditions are chosen so that they represent sufficiently large differences in the magnitude and phase of the nominal reflection coefcient within the frequency range of the test (up to 500 Hz), with the lower flow resistivity boundaries having smaller magnitudes but larger phase angles. This enable testing of the validity of the different implementations over a wide range of values. The results calculated by the FDTD using the different approximation and implementations of the boundary conditions are shown in Figure 5 for the differents cases. In the figure, the different implementations are identified by abbreviations in the form of *XXX-YYY-ZZ*, where *XXX* denotes the material data type (impedance or reflection coefficient) used to represent the boundary condition, *YYY* denotes the approximation method (2DOF or minimum phase) used to construct the *z*-domain filter, and *ZZ* denotes the type of relationship (impedance equation or reflection equation) used in the FDTD to implement the boundary condition. For example, the abbreviation NI-2DOF-I corresponds to the implementation using the boundary impedance data (**NI**) as the starting point, which is then approximated by a 2-DOF (**2DOF**) representation (Eqn.(7)) and transformed into a filter (Eqn.(10)) via the z-transform, and finally implemented in the FDTD update equation through the impedance (**I**) equation (Eqns. (11) and (12)).

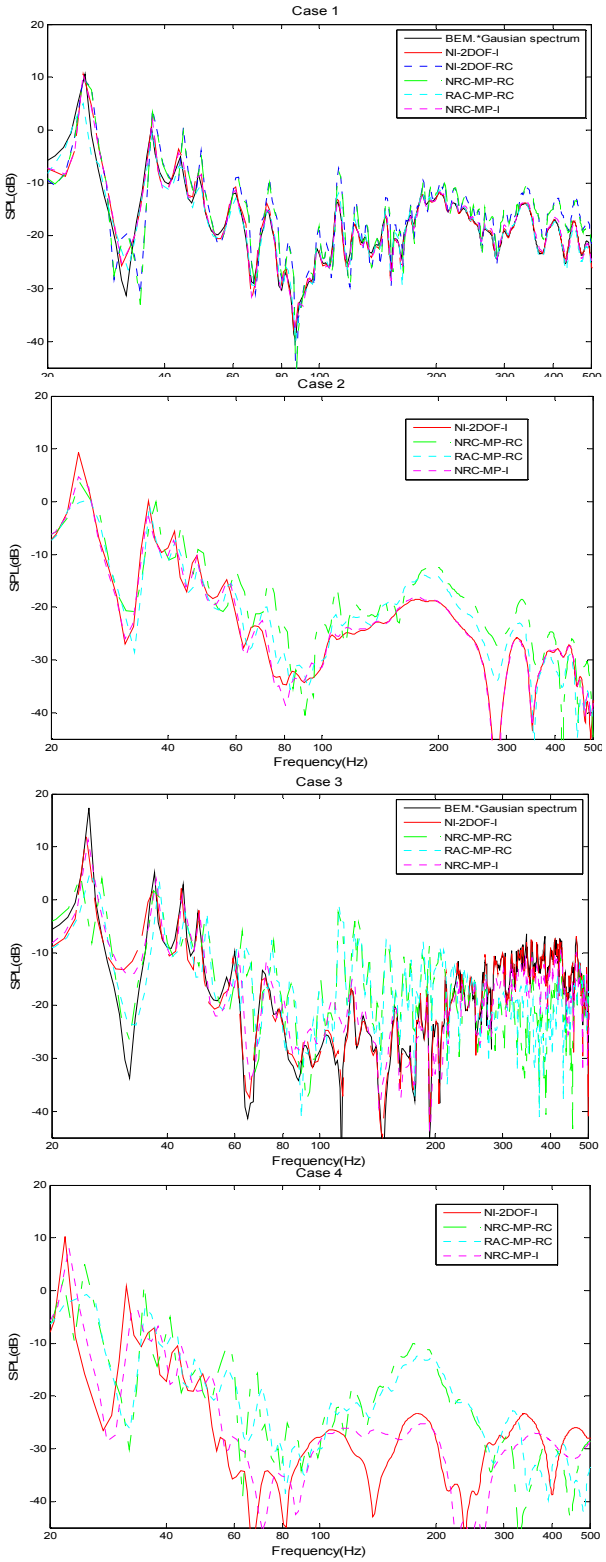

Figure 5 Results at R4 in the four different listening room settings (DATA TYPE - NI: Normal impedance; NRC: Normal reflection coefficient; RAC: Random incidence absorption coefficient. APPROXIMATION METHODS - 2DOF: two degree of freedom; MP: Minimum phase filter. IMPLEMENTATION APPROACHES - I: Impedance approach; RC: Reflection coefficient approach).

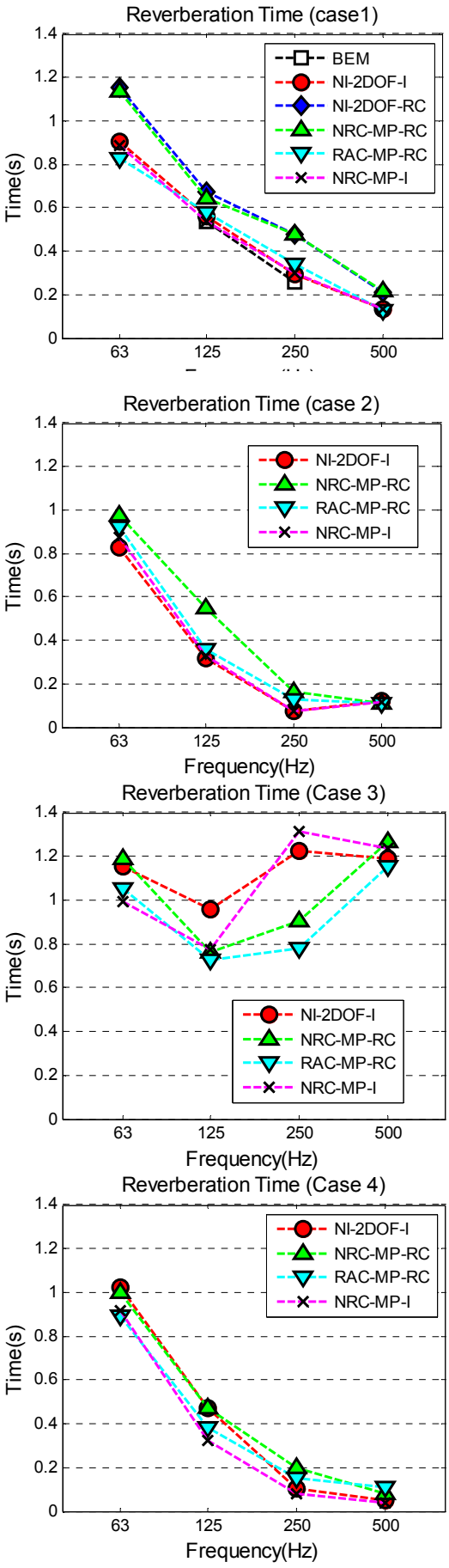

Figure 6 Reverberation time at R4 in four different listening room settings

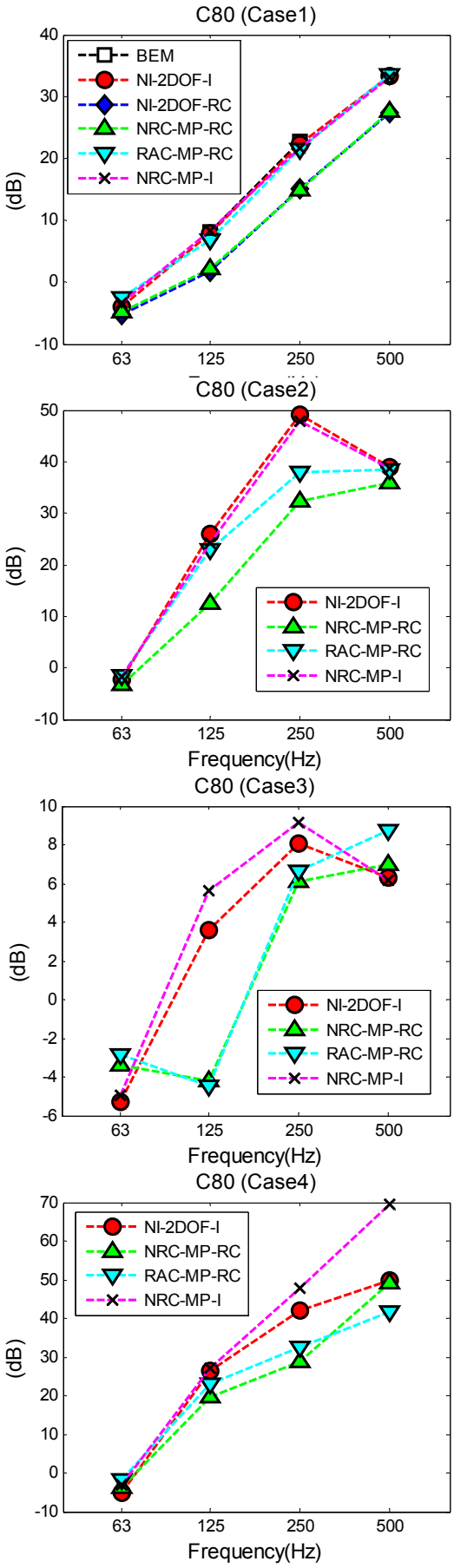

Figure 7 C_{80} at R4 for four different listening room settings

The result for Case1 in Figure 5 shows that when the boundary barely has phase changes, the impedance and reflection coefficient approaches with random incident absorption coefficient have similar accuracy when compared to the theoretically exact BEM. In addition, even when there are large phase changes (Case4), the reverberation time (Fig.6) calculated using a boundary condition approximated from the random incidence absorption coefficient is still within the difference limens. However, it was found that if there is not enough random incident waves onto the boundary (Case3), this approximate boundary condition based on absorption coefficient does not give accurate results.

The results on C_{80} in Fig.7 show similar trend. The error is largest when the sound field is least random (Case 3). otherwsie the implementation using the random incidence absorption coefficient as the starting material data gives farily reasonable results.

CONCLUSIONS

Several combinations of approximations and implementing methods for the frequency dependent boundary conditions were tested and compared against each other. When the effect of the hard source is appropriately removed, the result of the FDTD method showed very good agreement with the boundary element method. In particular, the results shows that when there are enough random incident waves into the boundaries in the room, the absorption coefficient can be used to obtain a suitable time domain boundary condition for FDTD calculations.

REFERENCES

[1] Drumm, I. and Lam, Y. W. (2007), Development and assessment of a finite difference time domain room acoustic prediction model that uses hall data in popular formats, INTER-NOISE, Istanbul, Turkey, August.

[2] Jeong, H., Drumm, I., Horner, B. and Lam, Y. W. (2007), The modeling of frequency dependent boundary conditions of concert hall acoustics, 19th International congress on acoustics, Madrid, September.

[3] Sakamoto, S., Nagamoto, H. and Asakura, T. (2007), Treatment of absorbing boundary condition for FDTD analysis on room acoustics, 19th International congress on acoustics, Madrid, September.

[4] Kowalczyk, K and Maarten V. W. (2008), Modeling frequency dependent boundaries as digital impedance filters in FDTD and K-DWM Room Acoustics Simulations, JAES Volume 56 Issue 7/8, July/August.

[5] Rienstra, S. W (2005), Impedance models in Time Domain, Eindhoven University of Technology, Messiaen Project.

[6] Özyörük, Y. and Long, L. N. (1996), A Time-Domain Implementation of Surface Acoustic Impedance Condition with and without Flow. American Institute of Aeronautics and Astronautics, Inc.

[7] Botteldooren, D. (1995), Finite-Difference Time-Domain Simulation of Low-Frequency Room Acoustic Problems. J. Acoust. Soc. Am. 98, No6.

[8] Maloney, J. C. and Cummings, K.E. (1995), Adaptation of FDTD Techniques to Acoustic Modelling, Proc. of the 11 Annual Reviews of Progress in Applied Computational Electromagnetics, Monterey, CA, vol.2 pp. 724-731.

[9] Taflove, A. and Hagness, S.C. Computational Electrodynamics: The Finite-Difference Time-Domain Method, 2nd Ed. (Artech House, Norwood MA, 2000).

[10] Lam, Y. W. (2005), Issues for computer modelling of room acoustics in non-concert hall settings, Acoust. Sci. & Tech. 26, 145–155

[11] Olesen, S. K. (1997), Low frequency room simulation using finite difference equations, AES Convention #102, Preprint 4422, March.

[12] Delany, M. E. and Bazley, E. N. (1970), Acoustical properties of fibrous absorbent materials, Appl. Acoust. 3, 105-116.